Carbon 116 (2017) 223–231

Contents lists available at ScienceDirect

Carbon

journal homepage: www.elsevier.com/locate/carbon

Controllable nanoscale engineering of vertically aligned MoS_2 ultrathin nanosheets by nitrogen doping of 3D graphene hydrogel for improved electrocatalytic hydrogen evolution

Li Zhao [a], Congcong Hong [a], Liangxu Lin [b], Huaping Wu [c], Yewang Su [d], Xiaobo Zhang [a], Aiping Liu [a, d, *]

[a] Center for Optoelectronics Materials and Devices, Zhejiang Sci-Tech University, Hangzhou 310018, China
[b] College of Engineering, Mathematics and Physical Sciences, University of Exeter, Exeter EX4 4QL, UK
[c] Key Laboratory of E&M (Zhejiang University of Technology), Ministry of Education & Zhejiang Province, Hangzhou 310014, China
[d] State Key Laboratory of Nonlinear Mechanics, Institute of Mechanics, Chinese Academy of Sciences, Beijing 100190, China

ARTICLE INFO

Article history:
Received 31 October 2016
Received in revised form
25 January 2017
Accepted 5 February 2017
Available online 6 February 2017

ABSTRACT

Three-dimensional (3D) porous molybdenum disulfide/nitrogen-doped reduced graphene oxide (MoS_2/N-rGO) hydrogels were fabricated through a facile and controllable one-pot hydrothermal method. The nanosized MoS_2 ultrathin nanosheets were uniformly and vertically dispersed on the rGO framework after nitrogen incorporation. The incorporated nitrogen in rGO played a key role for nano-scaling of MoS_2 due to the protonation at pyridinic N-doping sites on carbon surface. The vertically aligned edge of nanosized MoS_2 sheets, nitrogen incorporation of rGO and 3D network structure made the MoS_2/N-rGO highly efficient for hydrogen evolution reaction, with improved double-layer capacitance and turnover frequency, small onset overpotential of 119 mV, low Tafel slope of 36 mV·decade^{-1} and superior long-time catalytic stability.

1. Introduction

Electrochemical hydrogen evolution reaction (HER) is considered as one of the most promising techniques for developing clean and renewable energy resources [1–4]. Noble metals electrocatalysts based on platinum are hailed as the most efficient electrochemical catalysts for HER due to the exceptionally minimal overpotential closed to the thermodynamic potential for HER [5–8]. However, the high cost and low abundance prohibit their potential utilization of commercialization.

Great efforts in developing alternative abundant and cheap HER catalysts are focused on transition metal sulfides, especially the molybdenum disulfide (MoS_2) [2,9–11]. Theoretically, MoS_2 has comparable catalytic activity to Pt for HER due to its relatively low adsorption free energy for proton [12,13]. Nevertheless, the layer stacking induced by the Van der Waals force between individual layers limits its catalytic activity and further application in HER, since the catalytic activity of MoS_2 highly depends on the active exposed edges and electrical hopping between layers [14,15]. It is reported that vertically aligned nanosized MoS_2 with more exposed active edge sites and higher specific surface exhibited higher electrocatalytic activities than bulk MoS_2 [2,16–22]. Hence, one effective strategy to improve the edge ratio of MoS_2 is to construct vertically aligned morphology. Massive efforts have been committed to this purpose. For example, Cui's group [17] prepared MoS_2 thin films with vertically aligned to maximally expose the edges grown on flat substrates by chemical vapor deposition method and favor the HER performances. Li et al. [21] synthesized vertically standing MoS_2 nanosheets *via* a similar procedure, gave improved exchange current density in compare with bulk MoS_2. However, the extremely low electrical conductivity of MoS_2 nanostructure, especially along the adjacent interlayers hampers the electron transfer for highly efficient HER. Further improvement of the HER performance of MoS_2 is possible by introducing highly conductive substrate material such as nanoporous carbon [23], carbon nanotube (CNT) [24–26], nanoporous metal [27] or graphene [28–31] to facilitate electron

* Corresponding author. Center for Optoelectronics Materials and Devices, Zhejiang Sci-Tech University, Hangzhou 310018, China.
E-mail address: liuaiping1979@gmail.com (A. Liu).

http://dx.doi.org/10.1016/j.carbon.2017.02.010
0008-6223/

transfer process at the interfaces. Recently, three-dimensional (3D) conductive graphene networks, a framework of interconnected graphene sheets, has been considered as an effective substrate for loading and confining MoS_2 for HER performance improvement due to its prominent properties including large specific surface area, strong mechanical strength, remarkable electronic conductivity and fast mass and electron transport kinetics [32–36]. Moreover, heteroatom doping has become a promising approach to further improve properties of carbon material for various applications, such as supercapacitors, Li-ion batteries, oxygen reduction reaction and electrocatalysis [24,37–39]. For example, Li et al. [24] reported a hybrid of N-doped CNT and amorphous MoS_x, which demonstrated enhanced HER activity due to the synergistic effect from the dense catalytic sites at amorphous MoS_x surface and fluent charge transport along N-doped CNT surface. The N-doping could also effectively modulate the electronegativity of graphite carbon by offering excessive valence electrons to graphitic plane, maintaining high electroconductivity of composite materials as well as catalyst durability [40–42]. However, the study of N-doping effect on morphology and HER catalytic performance of MoS_2 sheets dispersed on 3D rGO frameworks is barely reported.

Herein, we demonstrated a one-step, solvent-assisted hydrothermal technique to easy fabricate vertically aligned MoS_2 ultrathin nanosheets decorated on 3D porous nitrogen-doped reduced graphene oxide (MoS_2/N-rGO) hydrogels. We explored how nitrogen doping, nitrogen content and reaction solvent affected the morphology and HER performance of MoS_2/N-rGO hydrogels. More important, we found that nitrogen incorporation in rGO played a key role for the nano-scaling of MoS_2 vertically dispersed on rGO due to the protonation at pyridinic N-doping sites on carbon surfaces. The vertically aligned edges of nanosized MoS_2 ultrathin nanosheets, nitrogen incorporation of rGO with high conductivity and 3D network structure of hydrogels favored the MoS_2/N-rGO catalysts to be efficient HER catalyst, with a small onset overpotential of 119 mV, a low Tafel slope of 36 mV·decade^{-1} and superior long-time catalytic stability.

2. Experimental

2.1. Materials and regents

Graphite and ammonium tetrathiomolybdate ($(NH_4)_2MoS_4$) were obtained from Alfa Aesar. Potassium permanganate ($KMnO_4$), sulfuric acid (H_2SO_4, 98%), sodium hydroxide (NaOH) and sodium nitrate ($NaNO_3$) were purchased from Sinopharm Chemical Reagent Co. Ltd. N,N-dimethylformamide (DMF) and ammonium hydroxide solution ($NH_3·H_2O$) were obtained from Shanghai Chemical Reagent Company. Deionized (D.I.) water was obtained from Millipore Milli-Q purification system (18.2MΩ·cm). All reagents were of analytical grade and used without further purification.

2.2. Synthesis of 3D MoS_2/N-rGO hydrogels

The 3D MoS_2/N-rGO hybrid hydrogels were prepared by a simple one-step hydrothermal process. Graphene oxide (GO) was prepared by a modified Hummers' method [43]. Briefly, 60 mg of $(NH_4)_2MoS_4$, 13 mL of mixed solvent of DMF and D.I. water (volume ratio of 2:1), 1.5 mL of GO aqueous (15.5 mg·mL^{-1}) and 0.5 mL $NH_3·H_2O$ were adequately mixed to form a homogeneous solution under sonication. The reaction solution was transferred to a 25 mL Teflon-lined autoclave and kept in an oven at 200 °C for 8 h. The autoclave was cooled down to room temperature naturally and the resulting products was washed and filtrated with ethanol and D.I. water until the pH of the solution close 7 and freeze-dried overnight. In order to explore the effect of $NH_3·H_2O$ amount on the morphology and catalytic performance of MoS_2/N-rGO hydrogel, the amount of $NH_3·H_2O$ in the suspension was changed from 0.25 mL to 3 mL with the corresponding samples named as MoS_2/N-r$GO_{0.25}$, MoS_2/N-r$GO_{0.5}$, MoS_2/N-r$GO_{0.75}$, MoS_2/N-rGO_1, MoS_2/N-rGO_2 and MoS_2/N-rGO_3, respectively. The MoS_2/rGO hydrogel prepared without the $NH_3·H_2O$ addition was synthesized *via* the same hydrothermal method as comparison. To explore the influence of pH on the morphology of MoS_2/N-rGO hydrogels, $NH_3·H_2O$ was replaced by different amounts of NaOH (0.5 mol) with the adjustment of the same pH value to $NH_3·H_2O$-including system under the same conditions. The effect of solvent for the morphology and catalytic performance of MoS_2/N-rGO hydrogels were also investigated by replacing the mixed solvent of DMF and D.I. water by pure D.I. water or DMF in the reaction process. In addition, pristine MoS_2 nanosheets and N-rGO hydrogel (0.5 mL $NH_3·H_2O$ used in the suspension) were synthesized under the same conditions without the addition of GO and $(NH_4)_2MoS_4$, respectively.

2.3. Characterization

The morphology and structure of MoS_2/N-rGO hydrogels were observed by a field emission scanning electron microscope (FESEM, Hitachi S4800) and a transmission electron microscopy (TEM, Hitachi H-7650) equipped with an energy-dispersive X-ray spectroscopy (EDS) at an acceleration voltage of 200 kV. High-resolution TEM (HRTEM) images were obtained at an operating voltage of 300 kV. X-ray diffraction (XRD) measurements were performed on an X-ray diffractometer (Bruker AXS D8) using the Cu Ka radiation ($\lambda = 0.15418$ nm) with the 2θ scan from 5° to 80° at a step of 0.02°. Raman spectra were recorded on a Thermo Fisher DXR Raman spectrometer with a He–Ne laser ($\lambda = 632.8$ nm). Fourier transform infrared (FTIR) spectroscopy was obtained on a Nicolet Avatar 370 spectrometer. The thermal gravimetric analysis (TGA) was conducted on a TA Q500 Instrument under flowing air at a heating rate of 10 °C min^{-1}. X-ray photoelectron spectroscopy (XPS) was collected by an X-ray photoemission spectrometer (KRATOS AXIS ULTRA-DLD).

For electrode preparation, 2 mg of a given catalyst sample and 80 μL Nafion solution (5 wt%) were dispersed in 1 mL water-ethanol solution (volume ratio of 3:1) and sonicated for 30 min to form a homogeneous ink. Then 5 μL portion of the resulting solution was drop-cast onto the glass carbon electrode (GCE) with 3 mm in diameter (loading ~0.14 mg·cm^{-2}) and dried in the room temperature. Linear sweep voltammetry (LSV) measurement was conducted in a nitrogen purged 0.5 M H_2SO_4 solution with the scan rate of 5 mV·s^{-1}. The stability tests of catalyst were obtained at a sweep rate of 100 mV·s^{-1} for 2000 cycles with each cycle started at +0.10 V and ended at −0.4 V. Electrochemical impedance spectroscopy (EIS) was carried out in the same configuration at $\eta = 170$ mV from 10^6 to 0.01 Hz with an amplitude of 5 mV. All electrochemical measurements were performed on a CHI 660D electrochemical work station (Shanghai Chenhua Instrument Co., China) with a standard three-electrode cell at room temperature. A GCE was used as the working electrode, a saturated calomel electrode (SCE) and a graphite rod were used as the reference electrode and counter electrode, respectively. The turnover frequency (TOF) and double-layer capacitance (C_{dl}) of catalysts were measured according to the method reported by previous work [5,44]. The potential transfer from SCE to reversible hydrogen electrode (RHE) was $E_{(RHE)} = E_{(SCE)} + 0.267$ V. All the potentials reported in our manuscript were calibrated to RHE. Current density referring to the geometric surface area of the GCE was used. All data were presented with iR compensation.

3. Results and discussion

3.1. Morphology and microstructure of MoS_2/N-rGO hydrogels

Fig. 1 shows the morphologies of different MoS_2/rGO hydrogels. The pure MoS_2 sample displays highly aggregated flower-like morphology with a size around 200 nm (Fig. 1a and b). With the addition of a certain amount of GO, the MoS_2/rGO hydrogel is obtained, showing a 3D porous framework constructed by interconnected lamellar nanosheets (Fig. 1c). The MoS_2 nanosheets covered in rGO layers present interconnected ripples with the lateral size from hundreds of nanometers to several microns (Fig. 1d). In order to clearly distinguish the MoS_2 sheets from the rGO wrinkles, the HRTEM image and corresponding element mapping of MoS_2/rGO hydrogel are shows in Fig. S1. It can be seen that the interconnected MoS_2 nanosheets are vertically aligned on the rGO surface, which have 6–10 layers with the interlayer spacing of 0.92 nm (larger than ~0.61 nm of pure 2H–MoS_2) by statistically analyzing from 20 TEM images (at least 40 lattice fringes of MoS_2 nanosheets), and the Mo and S elements under the background of C and O elements have an atomic ratio of 0.55 (*e.g.* $MoS_{1.8}$/rGO). When $NH_3 \cdot H_2O$ was added in the reaction system, the pore structure of MoS_2/N-rGO hydrogel is more homogeneous with the well-constructed pore size ranging from hundreds of nanometers to micrometers (Fig. 1e). The porous scaffold structure would be helpful for reducing transport limitation of the electrolyte and accelerating the transfer of protons and electrons [33,36]. To our surprise, the MoS_2 nanosheets with the lateral size of dozens of nanometers vertically adhered to the surface of N-rGO framework (Fig. 1f), which have more exposed active sites. Moreover, the TEM (Fig. 2a) and HRTEM (Fig. 2b) images show that the MoS_2 nanosheets on N-rGO surface have 4–6 layers with the interlayer spacing of 0.92 nm and abundant defects (Fig. 2b) by statistically analyzing from 20 TEM images (at least 40 lattice fringes of MoS_2 nanosheets). The elemental mapping images of the MoS_2/N-rGO during TEM characterization (Fig. 2c) suggest the uniform distribution of C, N, Mo and S elements and give an atomic ratio of 0.55 (Mo:S, *e.g.* $MoS_{1.8}$/rGO).

The XRD patterns of the as-prepared MoS_2, MoS_2/rGO and MoS_2/N-rGO composites are shown in Fig. 3(a). Pristine MoS_2 exhibits three characteristics peaks at about $2\theta = 9.3$, 32.2 and 56.5°, which can be assigned to the (002), (100) and (110) crystal planes of hexagonal MoS_2 (2H–MoS_2, JCPDS 37-1492), respectively. It is remarkable that the characteristics peaks of (002) crystallographic plane of the MoS_2 shift to 9.3°, corresponding to the interlayer spacing of about 0.92 nm. This could be derived from the disorder engineering and oxygen incorporation of MoS_2, as elaborately discussed in our previous report [45]. The peak at 18.3° is also a powerful evidence of enlarged interlayer spacing of MoS_2, as proposed by Xie et al. [4]. In addition, the (002) diffraction of rGO in N-rGO, MoS_2/rGO and MoS_2/N-rGO hydrogels at about 24.5° exhibits the interlayer distance about 0.34 nm, confirmed the successful reduction of GO to rGO [46]. The slight difference of (002) diffraction of MoS_2 between MoS_2 and MoS_2/rGO (or MoS_2/N-rGO) hydrogels could be the synergistic effect between MoS_2 nanosheets and rGO (or N-rGO) during hydrothermal process. The Raman spectrum of MoS_2 in Fig. 3(b) presents two characteristics peaks at 373 and 400 cm^{-1} for MoS_2/N-rGO hybrids, belonging to in-plane E^1_{2g} and out-of-plane A_{1g} along the c-axis vibrational modes of 2H–MoS_2, respectively [2,44]. The difference between these two dominant peaks (27 cm^{-1}) is smaller when compared to MoS_2/rGO (29 cm^{-1}) and pure MoS_2 (31 cm^{-1}), indicating that the N-doped rGO sheets can more effectively hinder the layer stacking of MoS_2 nanosheets along the C axis during the hydrothermal process than rGO [13,30], as shown in Fig. 2b and Fig. S1b. The characteristic peaks of rGO at 1327 and 1597 cm^{-1} (Fig. 3c) also reveal the D band (represents edges, disordered carbon and defects) and G band (corresponds to vibration of ordered sp^2-hybridized carbon) [47] with the relative intensity ratio I_D/I_G increasing from 0.97 for GO, to 1.49 for MoS_2/rGO and to 1.58 for MoS_2/N-rGO, indicating more disorderly stacked carbon sheets after the N-incorporation as well as the successful reduction of GO to rGO [48]. The FTIR spectrum of MoS_2/N-rGO composite (Fig. S2) appears two N–H peaks at 1558 and 1469 cm^{-1} [49], which derived from the increase of nitrogen functional groups on the surface of MoS_2/N-rGO composites.

The XPS was then carried out to investigate the composition and chemical bonding states of the samples. Fig. 4(a) shows the XPS full survey of N-rGO, MoS_2/rGO and MoS_2/N-rGO composites, which

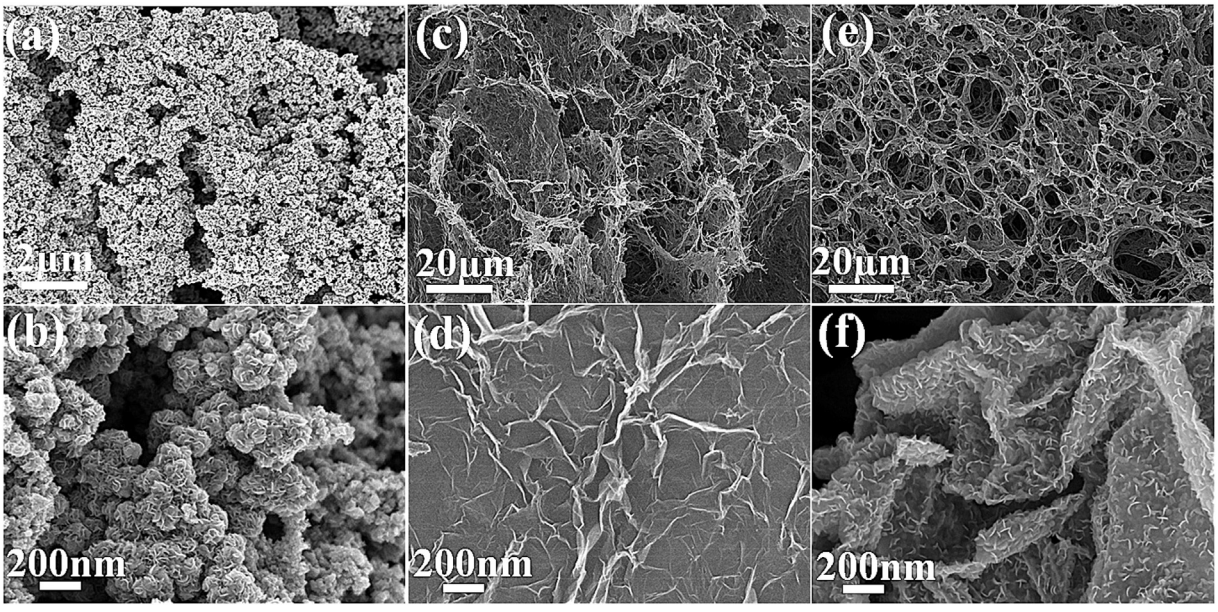

Fig. 1. Typical low- and high-magnification SEM images of (a,b) MoS_2, (c,d) MoS_2/rGO and (e,f) MoS_2/N-rGO catalysts.

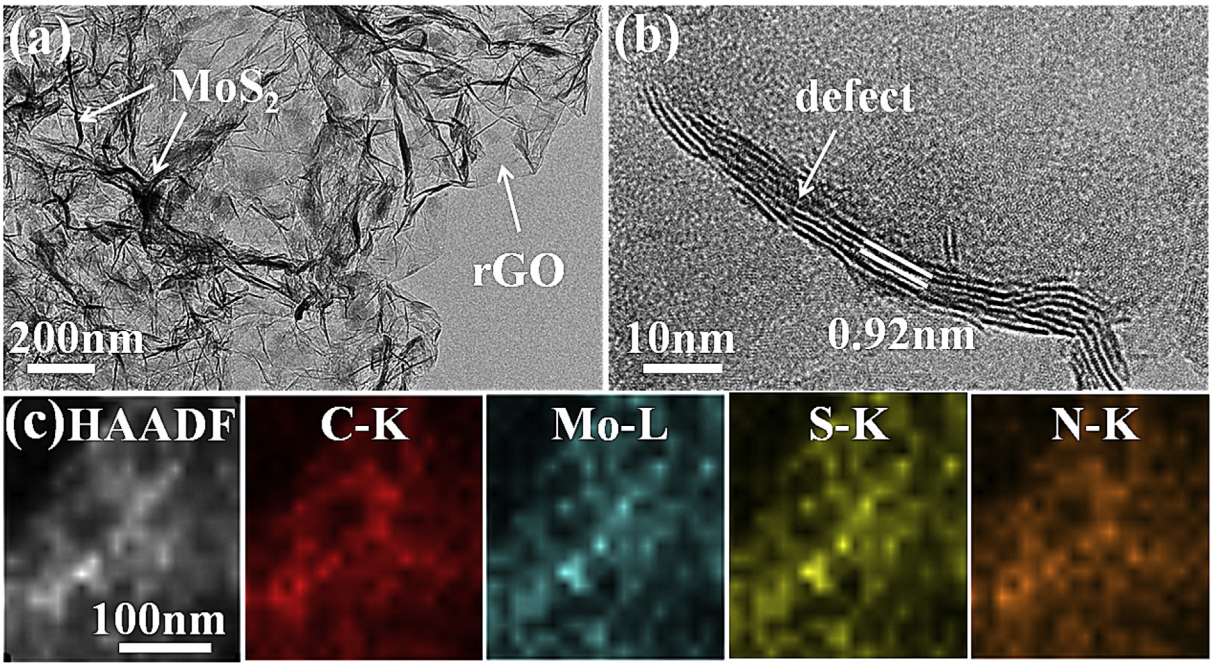

Fig. 2. (a) TEM and (b) HRTEM images of MoS_2/N-rGO catalysts. (c) High-annular dark-field scanning TEM image (HAADF-STEM) and corresponding element mapping of C, N, S and Mo. (A colour version of this figure can be viewed online.)

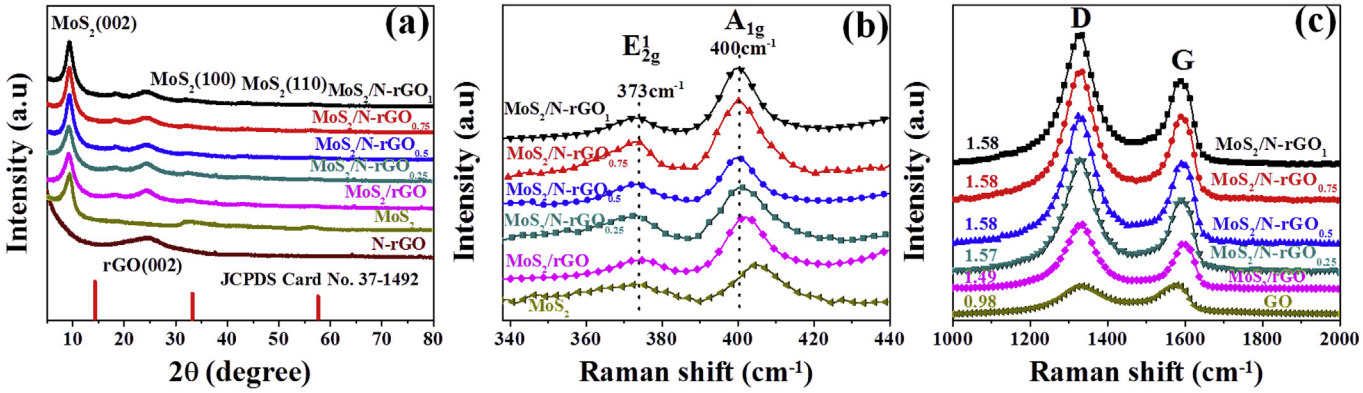

Fig. 3. (a) XRD pattern and (b)–(c) Raman shift of different MoS_2-based catalysts. (A colour version of this figure can be viewed online.)

reveals the presence of C, O, N, Mo and S elements in the MoS_2/N-rGO hybrid with the Mo/S atomic ratio of ~0.55, and is well consistent with the stoichiometric ratio of MoS_2 obtained from EDS results. The high-resolution C1s core-level spectrum of MoS_2/N-rGO hybrid (Fig. 4b) has a strong peak of C–C/C=C species (284.5 eV) and two relatively weak peaks of C–N (285.2 eV) and C–O (286.6 eV), which verifies the reduction of GO and the successful nitrogen doping in the 3D framework [50]. The Mo 3d spectrum in Fig. 4(c) displays two characteristic peaks at 228.8 (Mo 3d5/2) and 232.2 eV (Mo 3d3/2), indicating the Mo (IV) oxidation state for MoS_2 [50]. The peak at 226.3 eV could be indexed as S2s binding energy. The S2p spectrum (Fig. 4d) shows main doublet located at binding energies of 162.8 and 161.6 eV, which are attributed to the $S2p_{1/2}$ and $S2p_{3/2}$ orbitals, respectively. Meanwhile, the binding energy at 164.1eV suggests the existence of bridging disulfides S_2^{2-} and/or apical S^{2-} ligands related to the high HER activity [44]. The N1s spectrum in Fig. 4(e) can be deconvolved into four peaks centered at 398.2, 395.1, 400 and 401.7 eV, which are assigned to Mo3p, pyridinic N, pyrrolic N and graphitic N, respectively [48,49]. Though the N 1s peak partially overlaps with the strong $Mo3p_{3/2}$ signal, it still clearly displays multiple-peaked characteristic as shown in the N 1s spectrum of N-rGO without MoS_2 nanosheets (Fig. S3) [48]. Therefore, the N atoms are really successfully doped into the 3D rGO hydrogel with the nitrogen contents about 8.60 at.% for N-rGO (0.5 mL $NH_3 \cdot H_2O$ used in the suspension). Furthermore, by calculating the integral area of peak in N 1s spectrum, we speculate that the pyridinic N may be the main form of doped N in the rGO framework [24]. According to the study of Kim et al., the protonation of lone-pair electrons will be formed for pyridinic N-doping sites in the carbon materials [24] [51]. With the continuous increasing of $NH_3 \cdot H_2O$ amount in the reaction system, the integral areas of C–N peak in C1s spectrum and the pyridinic N peak in N1s spectrum are obviously enlarged, indicating the increased protonation at pyridinic N-doping sites in the composite. Additionally, the peak at 531.5 eV (C–O/O–C–N bond) in the O 1s spectrum (Fig. 4f) also shows the information related to doped N in the rGO.

To better explore the effect of nitrogen doping content on the

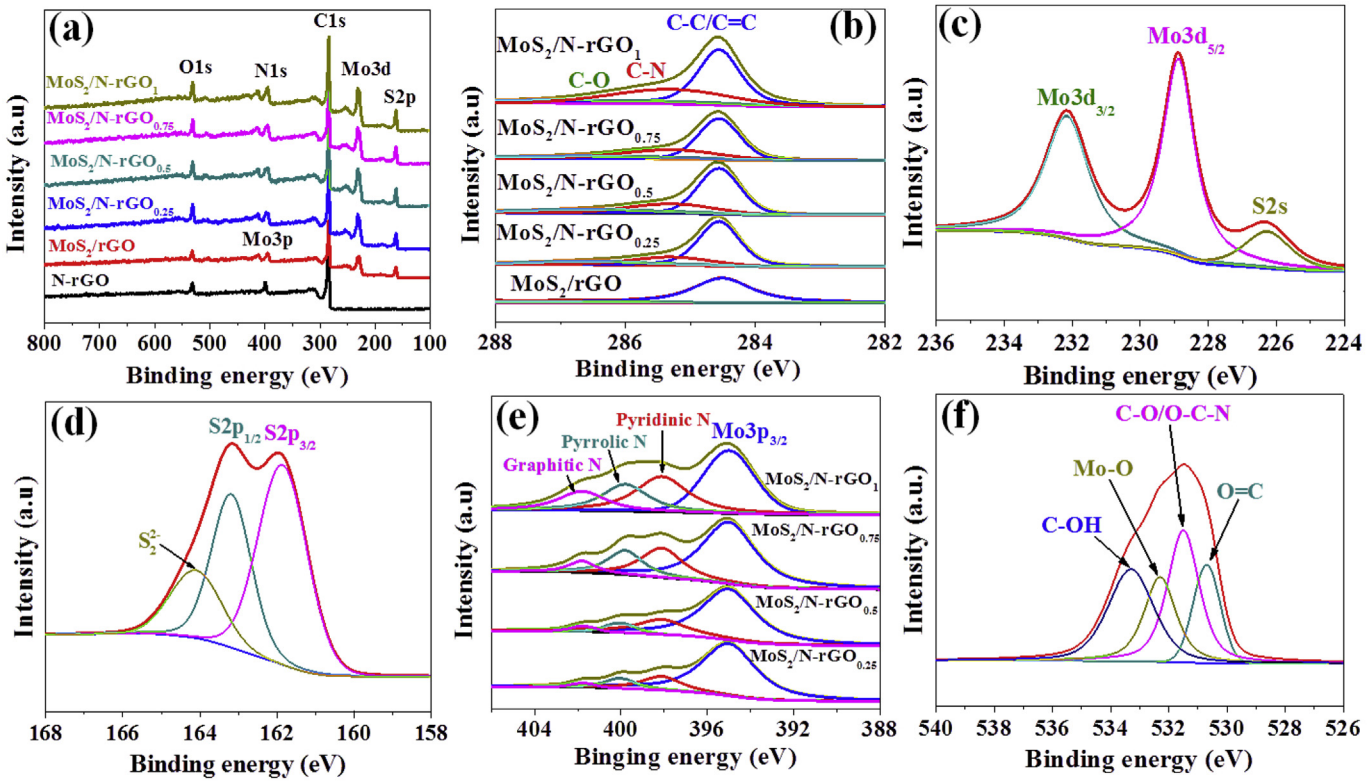

Fig. 4. XPS spectra of different MoS_2-based hybrids: (a) full-scan spectra of N-rGO, MoS_2/rGO and MoS_2/N-rGO, (b)–(f) high-resolution core-level spectra of (b) C 1s, (c) Mo 3d, (d) S 2p, (e) N 1s and (f) O 1s for MoS_2/N-rGO. (A colour version of this figure can be viewed online.)

morphology of 3D MoS_2/N-rGO hydrogel, reasonable experiments were designed. We change the amount of $NH_3 \cdot H_2O$ used in the reaction from 0.25 mL to 3 mL, respectively. When 0.25 mL $NH_3 \cdot H_2O$ is added in the reaction system, ultrathin vertically aligned MoS_2 nanosheets with the average lateral size about 80 nm are sparsely decorated on the N-rGO surface (Fig. 5a). Little change in the size but obvious increase in the density and exposed edges of MoS_2-sheet clusters can be observed when 0.5 mL $NH_3 \cdot H_2O$ is used (Fig. 1f). Further increasing the $NH_3 \cdot H_2O$ amount to 0.75 mL, the increscent dense MoS_2 sheets pack together (Fig. 5b) and ultimately form interconnected ripples with the lateral size about 300–400 nm when 1-mL $NH_3 \cdot H_2O$ added (Fig. 5c). When 2 mL and

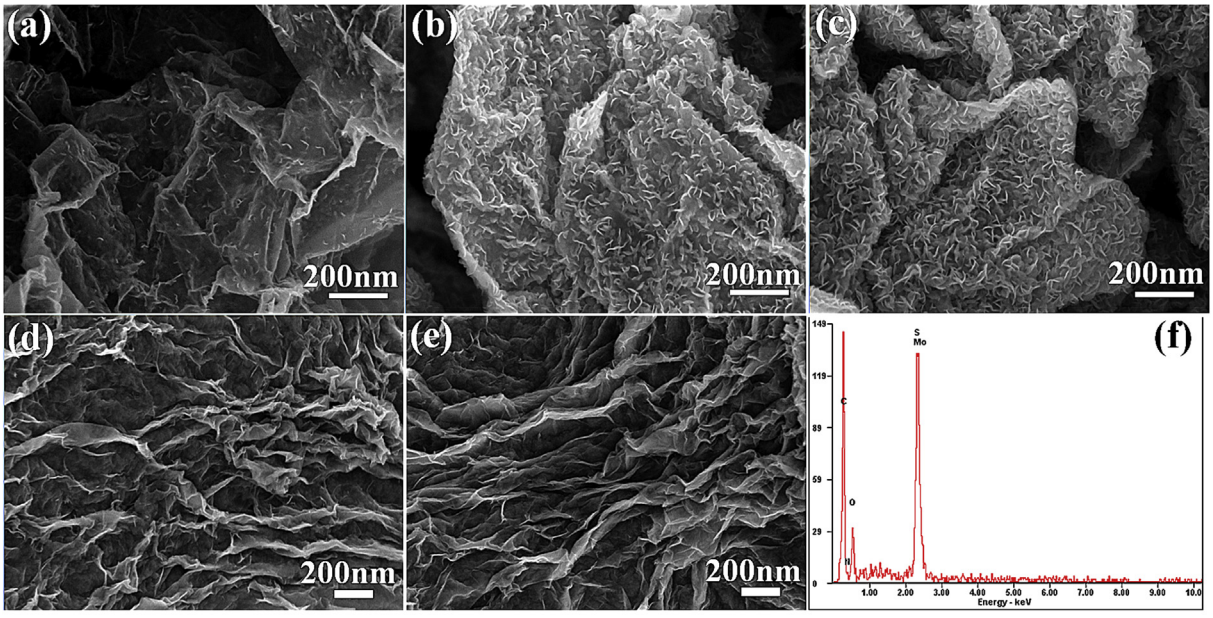

Fig. 5. SEM images and EDS result of MoS_2/N-rGO composites prepared with different $NH_3 \cdot H_2O$ addition amounts: (a) 0.25 mL, (b) 0.75 mL, (c) 1 mL, (d) 2 mL, (e) 3 mL and (f) 1 mL. (A colour version of this figure can be viewed online.)

3 mL $NH_3 \cdot H_2O$ are used, no obvious nanosized MoS_2 sheets can be observed due to the formation of interconnected ripples (Fig. 5d and e), indicating the existence of large amounts of MoS_2 sheets. The EDS results of different MoS_2-based hybrids (Fig. 5f and Table S1) indicate that the amounts of MoS_2 in the composite increases with the increasing $NH_3 \cdot H_2O$ (from 0.25 mL to 3 mL) in the reaction system, which is in agreement with the TGA results (Fig. S4). Furthermore, to investigate the solution pH influence on the morphology of MoS_2/N-rGO hydrogels, $NH_3 \cdot H_2O$ was replaced by different amounts of NaOH (0.5 mol) with the adjustment of the same pH value to $NH_3 \cdot H_2O$-including system under the same conditions (the pH value is 10.3, 10.8, 11.2 and 11.4, respectively, when 0.25, 0.5, 0.75 and 1 mL $NH_3 \cdot H_2O$ is used). The MoS_2/rGO hydrogels obtained in the NaOH-containing system (Fig. S5) present similar morphology to the one obtained in the non-$NH_3 \cdot H_2O$ system (Fig. 1c and d, the pH value is 6.8), and the morphology is almost unchanged with the continuous increase of NaOH in the reaction system, indicating that effects of pH (in the range from 10.3 to 11.4) on the MoS_2/rGO and MoS_2/N-rGO hydrogels is negligible. Our above investigations have suggested that the controllable nanoscale engineering of vertically aligned MoS_2 ultrathin nanosheets is carried out by the nitrogen doping of rGO hydrogel in the $NH_3 \cdot H_2O$-including system.

Based on all these information (SEM, EDS, XPS and Raman results), we propose that the increased N-doping sites on carbon surface played a key role for the formation of vertical aligned nanosized MoS_2. When the N element is incorporated into the carbon framework, three kinds of N bonding including pyridinic N, pyrrolic N and graphitic N might be formed. Among these, the pyridinic N-doping sites have the lone-pair electrons, which are easy to form the protonation according to the study of Kim et al. [24]. The protonated doping sites could attract the thiomolybdate anions (MoS_4^{2-}) of the $(NH_4)_2MoS_4$ precursor by the electrostatic attraction and serve as the nucleation sites for MoS_2 crystals, which could further decrease the nucleation barrier of MoS_2 and favor their growth along with the (002) crystallographic plane, resulting in nanosized MoS_2 sheets with abundant exposed edges (when compared to the ones anchored on undoped rGO surface), as shown in Scheme 1. However, excess N incorporation would provide superfluous nucleation sites for MoS_2, causing the agglomeration and reconnection of nanosized MoS_2 sheets, which is in turn unfavorable for efficient HER performance (decreases the number of exposed edge site and electrical conductivity of MoS_2/N-rGO, as discussion in the following part).

3.2. Electrochemical properties of MoS_2/N-rGO hydrogels

The HER performance of the samples were evaluated in a 0.5 M H_2SO_4 solution with a typical three-electrode system. As show in Fig. 6(a), with same amount (0.14 mg cm^{-2}) catalyst immobilized on GCE, the N-rGO shows almost no HER activity with a near horizontal line within the potential window. In contrast, the 3D MoS_2/N-r$GO_{0.5}$ hydrogel presents a superior HER activity with a small oneset potentials of 119 mV [obtained at a current density (j) of 0.1 mA·cm^{-2}] compared to many reported MoS_2/rGO hybrids (Table 1) [3,4,15,48]. Additionally, this hybrid exhibits a high j of 10 mA·cm^{-2} at 188 mV and 50 mA·cm^{-2} at 239 mV, respectively. The potentials are much lower than those achieved by MoS_2/rGO (226 mV and 275 mV) and pure MoS_2 (270 mV and 362 mV) at the same j. Tafel slop is the intrinsic property of electrocatalyst, which is associated with the reaction pathway and the adsorption type of H_2 evolution, and can be obtained by fitting the linear portions of the Tafel plots based on Tafel equation to quantitatively analyze the kinetics of HER [6,52]. As shown in Fig. 6(b), the Tafel slop of MoS_2/N-r$GO_{0.5}$ hybrids is 36 mV·$decade^{-1}$, which is lower than many reported MoS_2-based catalysts in Table 1 [2–4,15,25,48], indicating that the Volmer-Tafel reaction mechanism dominates during the HER process, and the Tafel reaction acts as the rate-limiting step [52,53]. In order to better explore the kinetics at the electrode/electrolyte interface during the HER process, we also performed the EIS analysis. A low Ohmic series resistance of the system (R_s, which is dependent on the intercept of the semicircle on the real axis, as shown in Fig. 6c) indicates excellent conductivity of electrolyte. Owing to the strong electronic interaction between MoS_2 nanosheets and N-rGO scaffold with high conductivity, the charge transfer resistance (R_{ct}) of MoS_2/N-r$GO_{0.5}$ composite (~6.5 Ω) is lower than the pure MoS_2 (~7.8 Ω) and MoS_2/rGO composite (~7.2 Ω), confirming that both nitrogen incorporation in rGO and rGO hybrid structure increase charge transfer of the catalyst for HER [15,24]. Notice that the R_{ct} of MoS_2/N-r$GO_{0.5}$ is lower than that of N-rGO (synthesized under the same conditions without the addition of $(NH_4)_2MoS_4$). Our SEM result shows that the N-rGO hydrogel exhibits large lamellar structure rather than a

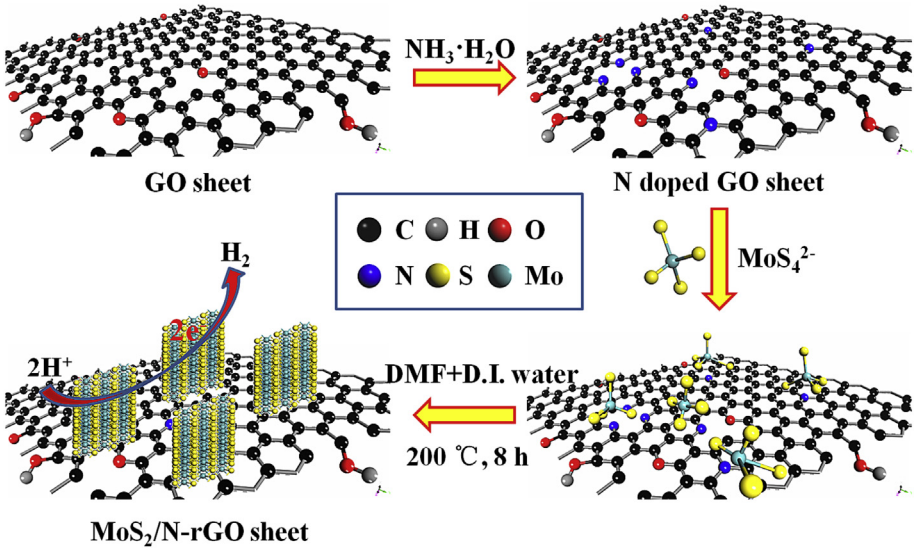

Scheme 1. Diagram shows the growth of vertically aligned nanosized MoS_2/N-rGO catalysts.

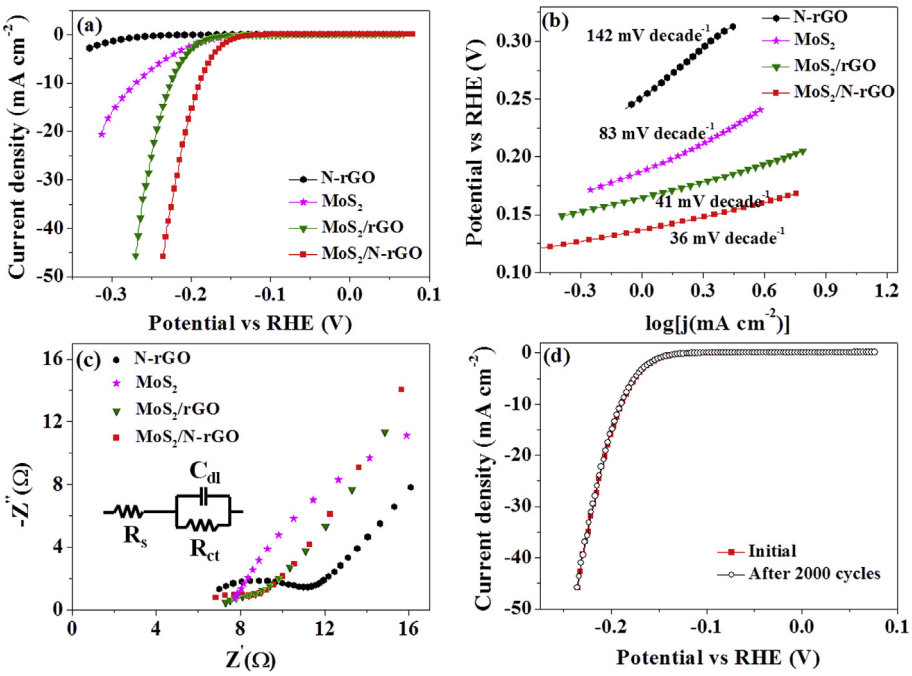

Fig. 6. (a) Polarization curves, (b) corresponding Tafel plots, and (c) EIS Nyquist plots of various catalysts modified electrode in a 0.5 M H_2SO_4 solution at 5 mV·s^{-1}. The inset in (c) is the equivalent model of system. (d) Stability test for MoS_2/N-rGO hydrogel in a 0.5 M H_2SO_4 solution at a scan rate of 50 mV·s^{-1}. (A colour version of this figure can be viewed online.)

Table 1
A brief summary of HER performance from various MoS_2 or MoS_2/rGO composites.

Sample	Mass loading (mg·cm^{-2})	Onset potential[a] (mV)	Tafel slope (mV·decade^{-1})	Reference
Defect-rich MoS_2 nanosheets	0.285	120	50	[3]
O-doped MoS_2 nanosheet	0.285	120	55	[4]
MoS_2/rGO	0.2	140	41	[15]
MoS_2/rGO	0.285	100	41	[2]
MoS_2/CNT	0.136	90	44.6	[25]
MoS_2/N-doped graphene	0.707	236	230	[48]
MoS_2/N-rGO	0.14	119	36	This work

[a] Onset overpotential was obtained at current density of 0.1 mA·cm^{-2}.

porous structure (Fig. S6), which is disadvantageous for reducing transport limitation of the electrolyte and therefore retards the transfer of protons and electrons. Besides, the MoS_2/N-r$GO_{0.5}$ catalyst exhibits excellent durability with negligible degradation in the current density even after continuous 2000 cycles (Fig. 6d) under acid condition. By contrast, the MoS_2/rGO catalyst without N-doping displays an obvious decrease in the current density after 1000 cycles (Fig. S7). Such excellent HER performance and durability of MoS_2/N-r$GO_{0.5}$ catalyst can be rationalized as follows: i) the introduction of N-doped sites in rGO provides more active nucleation sites for MoS_2, forming nanosized MoS_2 sheets with increased vertical edge ratio and defects and giving more exposed Mo edges to participate catalytic process; ii) the incorporated N improves the conductivity of rGO sheets, promoting fast electron transfer at the MoS_2/N-r$GO_{0.5}$ interface and electron mobility along the N-rGO nanosheets; iii) 3D hydrogel framework not only provides convenient channel for electrons and protons transfer, shortens the transfer path of charge carriers to active centers, but also decreases the volume change during the long-time test in acid media, favoring the catalyst better HER activity and stability.

The decisive influence of N incorporation on the HER catalytic activity is further confirmed by exploring the exposed active sites of the catalysts *via* two important parameters, namely C_{dl} and TOF. The C_{dl} characterizes the effective active surface area (EASA) and rich exposed active sites of catalysts and can be calculated by the scanning area of cyclic voltammetry (CV) curves at the Non-Faraday region (Fig. S8, see Supporting Information for more information) [5]. It can be clearly seen that the MoS_2/N-r$GO_{0.5}$ shows the largest C_{dl} ~31.02 mF·cm^{-2} than other MoS_2-based catalysts (Fig. 7a), which is 3 times larger than that of pristine MoS_2 (8.92 mF·cm^{-2}) and 2 times larger than that of MoS_2/rGO catalyst (15.65 mF·cm^{-2}). This value is rather competitive considering the low mass loading when compared to previously reported MoS_2-based catalysts, such as defect-rich MoS_2/rGO nanosheets (6.045 mF·cm^{-2}) [30], MoS_x/PP-CFP films (4.13 mF·cm^{-2}) [54] and AS-rich MoS_2 nanospheres (27.5 mF·cm^{-2}) [55]. Additionally, the calculated TOF, which is usually used to determine the active sites of the catalyst (Fig. S9, see Supporting Information for more information) [44,56], confirms a better catalytic ability for MoS_2/N-r$GO_{0.5}$ catalyst (TOF = 0.89 s^{-1} at an overpotential of 240 mV) when compared to the MoS_2/rGO (TOF = 0.51 s^{-1}) and pure MoS_2 (TOF = 0.29 s^{-1}) at the same overpotential (Fig. 7b). Therefore, the vertically aligned nanosized structure of MoS_2, nitrogen incorporation of rGO and 3D network structure have led to excellent HER performances of the MoS_2/N-r$GO_{0.5}$ composite.

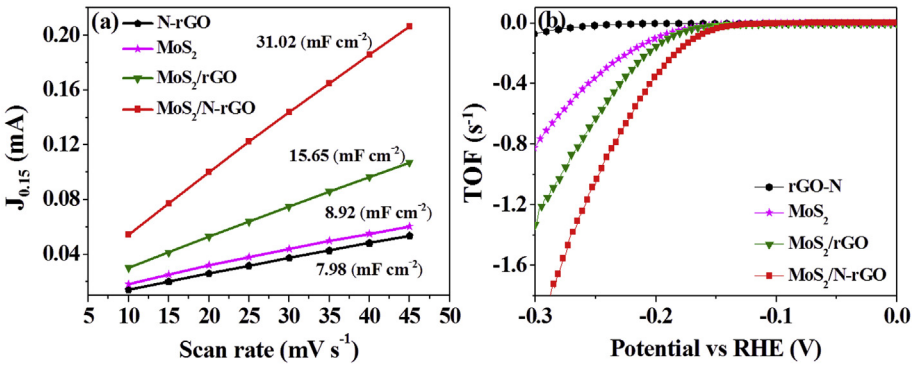

Fig. 7. (a) Relations of difference between anodic and cathodic currents at 0.15 V (*vs* RHE) ($J_{0.15} = J_a$-J_c) with various scan rates from 10 mV·s^{-1} to 45 mV·s^{-1}. The slope is double C_{dl}. (b) Turnover frequency (TOF) of various catalysts in a 0.5 M H_2SO_4 solution at a scan rat of 50 mV·s^{-1}. (A colour version of this figure can be viewed online.)

However, excess N incorporation and 3D hydrogel-structure destruction cause the agglomeration and reconnection of MoS_2 sheets, sacrificing the catalytic active sites and electrical conductivity (electron hopping between layers). As shown in Fig. S10, with the increase of $NH_3 \cdot H_2O$ amount added in the reaction system, the HER performance, C_{dl} and R_s show a first increased and then decreased trend, and the optimal behavior is obtained in MoS_2/N-$rGO_{0.5}$ hydrogel. Therefore, the proper N-doped sites can efficiently restrict the growth of MoS_2 nanosheets for excellent electrocatalytic activities. Excess N concentration caused by using large amount of $NH_3 \cdot H_2O$ (2 and 3 mL) in the precursor (Table S1) would result in the reconnection of nanosized MoS_2 sheets and decrease the electrical conductivity and charge transfer resistance of MoS_2/N-rGO (Fig. S10), which degrades the HER performance of catalysts. We also probe the solvent effect on the hydrogel structure and HER activity of MoS_2/N-$rGO_{0.5}$ hybrid. When only DMF was used as the solvent in the hydrothermal reaction (GO was freeze-dried before used), the hybrid cannot self-assemble into 3D porous hydrogel structure (Fig. S11a and b). When pure D.I. water was used as the solvent under the similar conditions, despite the 3D porous structure remained, no homogeneous nanosized MoS_2 sheets with well-constructed pore size were obtained (Fig. S11c and d), and the HER performance degenerated (Fig. S12). Therefore, the proper proportion of DMF and water is important to construct a 3D porous framework which benefits the fast diffusion of electrolyte to active centers and accelerates electron transfer.

4. Conclusions

In summary, we have successfully synthesized vertically aligned MoS_2 ultrathin nanosheets decorated on 3D porous nitrogen-doped reduced graphene oxygen (N-rGO) hydrogel using a facile solvothermal approach. Thanks to the N-doping in the rGO, resulting in the formation of vertically aligned nanosized MoS_2 sheets with abundant exposed edges and rich defects. Moreover, 3D porous N-rGO hydrogel proves a good conductive skeleton, which accelerates the transportation of electrons and electrolyte during the HER process, favoring the MoS_2/N-rGO hydrogel excellent HER activity with a low Tafel slope of 36 mV·decade^{-1}, a small onset potential of −0.119 V, and superior long-time catalytic stability. What is more astonishing is that the dominant Turnover frequency (0.89 s^{-1}, at 240 mV) and high double layer capacitance (31.02 mF·cm^{-2}) can be obtained with the low mass loading, which are all much higher than previously reported MoS_2-based catalysts. This work successfully validates a simple-yet-effective synthesis method related to controllable nanoscale engineering of MoS_2 ultrathin nanosheets, which may provide promising candidates for cost-effective electrocatalysts for future commercial application.

Acknowledgments

This work was supported by the National Natural Science Foundation of China (Nos. 51572242, 11672269 and 11372280), the Zhejiang Provincial Natural Science Foundation of China (No. LY16E020011), the Program for Innovative Research Team of Zhejiang Sci-Tech University (No. 15010039-Y) and the Opening Fund of State Key Laboratory of Nonlinear Mechanics.

Appendix A. Supplementary data

Supplementary data related to this article can be found at http://dx.doi.org/10.1016/j.carbon.2017.02.010.

References

[1] Y.D. Hou, B.L. Abrams, P.C.K. Vesborg1, M.E. Björketun, K. Herbst, L. Bech, et al., Bioinspired molecular Co-catalysts bonded to a silicon photocathode for solar hydrogen evolution, Nat. Mater. 10 (2011) 434–438.
[2] Y.G. Li, H.L. Wang, L.M. Xie, Y.Y. Liang, G.S. Hong, H.J. Dai, MoS_2 nanoparticles grown on graphene: an advanced catalyst for the hydrogen evolution reaction, J. Am. Chem. Soc. 133 (2011) 7296–7299.
[3] J.F. Xie, H. Zhang, S. Li, R.X. Wang, X. Sun, M. Zhou, et al., Defect-rich MoS_2 ultrathin nanosheets with additional active edge sites for enhanced electrocatalytic hydrogen evolution, Adv. Mater. 25 (2013) 5807–5813.
[4] J.F. Xie, J.J. Zhang, S. Li, F. Grote, X.D. Zhang, H. Zhang, et al., Controllable disorder engineering in oxygen-incorporated MoS_2 ultrathin nanosheets for efficient hydrogen evolution, J. Am. Chem. Soc. 135 (2013) 17881–17888.
[5] H.T. Wang, Z.Y. Lu, D.S. Kong, J. Sun, T.M. Hymel, Y. Cui, Electrochemical tuning of MoS_2 nanoparticles on three-dimensional substrate for efficient hydrogen evolution, ACS Nano 8 (2014) 4940–4947.
[6] X. Zou, Y. Zhang, Noble metal-free hydrogen evolution catalysts for water splitting, Chem. Soc. Rev. 44 (2015) 5148–5180.
[7] N.P. Dasgupta, C. Liu, S. Andrews, F.B. Prinz, P. Yang, Atomic layer deposition of platinum catalysts on nanowire surfaces for photoelectrochemical water reduction, J. Am. Chem. Soc. 135 (2013) 12932–12935.
[8] Z.X. Wu, J. Wang, L.L. Han, R.Q. Lin, H.F. Liu, H.L. Xin, et al., Supramolecular gel-assisted synthesis of double shelled Co@CoO@N–C/C nanoparticles with synergistic electrocatalytic activity for the oxygen reduction reaction, Nanoscale 8 (2016) 4681–4687.
[9] C. Tan, H. Zhang, Epitaxial growth of hetero-nanostructures based on ultrathin two-dimensional nanosheets, J. Am. Chem. Soc. 137 (2015) 12162–12174.
[10] L.X. Lin, N.H. Miao, Y. Wen, S.W. Zhang, P. Ghosez, Z.M. Sun, et al., Sulfur-depleted monolayered molybdenum disulfide nanocrystals for super-electrochemical hydrogen evolution reaction, ACS Nano 10 (2016) 8929–8937.
[11] V. Kiran, D. Mukherjee, R.N. Jenjeti, S. Sampath, Active guests in the MoS_2/$MoSe_2$ host lattice: efficient hydrogen evolution using few-layer alloys of $MoS_{2(1-x)}Se_{2x}$, Nanoscale 6 (2014) 12856–12863.
[12] J.K. Nørskov, T. Bligaard, A. Logadottir, J.R. Kitchin, J.G. Chen, S. Pandelov, et al., Trends in the exchange current for hydrogen evolution, J. Electrochem. Soc. 152 (2005) 23–26.
[13] T.F. Jaramillo, K.P. Jørgensen, J. Bonde, J.H. Nielsen, S. Horch, I. Chorkendorff, Identification of active edge sites for electrochemical H_2 evolution from MoS_2

nanocatalysts, Science 317 (2007) 100–102.
[14] A.B. Laursen, S. Kegnæs, S. Dahl, I. Chorkendorff, Molybdenum sulfides-efficient and viable materials for electro – and photoelectrocatalytic hydrogen evolution, Energy Environ. Sci. 5 (2012) 5577–5591.
[15] X.L. Zheng, J.B. Xu, K.Y. Yan, H. Wang, Z.L. Wang, S.H. Yang, Space-confined growth of MoS_2 nanosheets within graphite: the layered hybrid of MoS_2 and graphene as an active catalyst for hydrogen evolution reaction, Chem. Mater. 26 (2014) 2344–2353.
[16] D.Y. Chung, S.K. Park, Y.H. Chung, S.H. Yu, Y.E. Sung, Edge-exposed MoS2 nano-assembled structures as efficient electrocatalysts for hydrogen evolution reaction, Nanoscale 6 (2014) 2131–2136.
[17] D.S. Kong, H.T. Wang, J.J. Cha, M. Pasta, K.J. Koski, J. Yao, et al., Synthesis of MoS_2 and $MoSe_2$ films with vertically aligned layers, Nano Lett. 13 (2013) 1341–1347.
[18] Y.F. Yu, S.Y. Huang, Y.P. Li, S.N. Steinmann, W.T. Yang, L.Y. Cao, Layer-dependent electrocatalysis of MoS_2 for hydrogen evolution, Nano Lett. 14 (2014) 553–558.
[19] Y. Yin, J.C. Han, Y.M. Zhang, X.H. Zhang, P. Xu, Q. Yuan, et al., Contributions of phase, sulfur vacancies, and edges to the hydrogen evolution reaction catalytic activity of porous molybdenum disulfide nanosheets, J. Am. Chem. Soc. 138 (2016) 7965–7972.
[20] M.A. Lukowski, A.S. Daniel, F. Meng, A. Forticaux, L.S. Li, S. Jin, Enhanced hydrogen evolution catalysis from chemically exfoliated metallic MoS_2 nanosheets, J. Am. Chem. Soc. 135 (2013) 10274–10277.
[21] H. Li, H.Q. Wu, S.G. Yuan, H. Qian, Synthesis and characterization of vertically standing MoS_2 nanosheets, Sci. Rep. 6 (2016) 21171.
[22] Y. Yang, H.L. Fei, G.D. Ruan, C.S. Xiang, J.M. Tour, Edge-oriented MoS2 nanoporous films as flexible electrodes for hydrogen evolution reactions and supercapacitor devices, Adv. Mater. 26 (2014) 8163–8168.
[23] Y. Liu, X.L. Zhou, T. Ding, C.D. Wang, Q. Yang, 3D architecture constructed via confined growth of MoS_2 nanosheets in nanoporous carbon derived from metal-organic frameworks for efficient hydrogen production, Nanoscale 7 (2015) 1–3.
[24] D.J. Li, U.N. Maiti, J. Lim, D.S. Choi, W.J. Lee, Y. Oh, et al., Molybdenum sulfide/N-doped CNT forest hybrid catalysts for high performance hydrogen evolution reaction, Nano Lett. 14 (2014) 1228–1233.
[25] Y. Yan, X.M. Ge, Z.L. Liu, J.Y. Wang, J.M. Lee, X. Wang, Facile synthesis of low crystalline MoS_2 nanosheet–coated CNTs for enhanced hydrogen evolution reaction, Nanoscale 5 (2013) 7768–7771.
[26] M. Khan, A.B. Yousaf, M.M. Chen, C.S. Wei, X.B. Wu, N.D. Huang, et al., Molybdenum sulfide/graphene-carbon nanotube nanocomposite material for electrocatalytic applications in hydrogen evolution reactions, Nano Res. 9 (2016) 837–848.
[27] Y.W. Tan, P. Liu, L.Y. Chen, W.T. Cong, Y. Ito, J.H. Han, et al., Monolayer MoS_2 films supported by 3D nanoporous metals for high-efficiency electrocatalytic hydrogen production, Adv. Mater. 26 (2014) 8023–8028.
[28] J.M. Zhang, L. Zhao, A.P. Liu, X.Y. Li, H.P. Wu, C.D. Lu, Three-dimensional MoS_2/rGO hydrogel with extremely high double-layer capacitance as active catalyst for hydrogen evolution reaction, Electrochim. Acta 182 (2015) 652–658.
[29] L. Liao, J. Zhu, X.J. Bian, L.N. Zhu, M.D. Scanlon, H.H. Girault, et al., MoS_2 formed on mesoporous graphene as a highly active catalyst for hydrogen evolution, Adv. Funct. Mater. 23 (2013) 5326–5333.
[30] Z.H. Deng, L. Li, W. Ding, K. Xiong, Z.D. Wei, Synthesized ultrathin MoS_2 nanosheets perpendicular to graphene for catalysis of hydrogen evolution reaction, Chem. Commun. 51 (2015) 1893–1896.
[31] C.B. Ma, X.Y. Qi, B. Chen, S.Y. Bao, Z.Y. Yin, X.J. Wu, et al., MoS_2 nanoflower-decorated reduced graphene oxide paper for high-performance hydrogen evolution reaction, Nanoscale 6 (2014) 5624–5629.
[32] Y.H. Chang, C.T. Lin, T.Y. Chen, C.L. Hsu, Y.H. Lee, W.J. Zhang, et al., Highly efficient electrocatalytic hydrogen production by MoS_x grown on graphene-protected 3D Ni foams, Adv. Mater. 25 (2013) 756–760.
[33] W.J. Zhou, K. Zhou, D.M. Hou, X.J. Liu, G.Q. Li, Y.H. Sang, et al., Three-dimensional hierarchical frameworks based on MoS_2 nanosheets self-assembled on graphene oxide for efficient electrocatalytic hydrogen evolution, ACS Appl. Mater. Interfaces 6 (2014) 21534–21540.
[34] Y.F. Zhao, X.Q. Xie, J.Q. Zhang, H. Liu, H.J. Ahn, K.N. Sun, et al., MoS_2 nanosheets supported on 3D graphene aerogel as a highly efficient catalyst for hydrogen evolution, Chem. Eur. J. 21 (2015) 1–6.
[35] Y.L. Liu, X. Chen, Mechanical properties of nanoporous graphene membrane, J. Appl. Phys. 115 (2014) 0021–8979.
[36] S.J. Xu, Z.Y. Lei, P.Y. Wu, Facile preparation of 3D MoS_2/$MoSe_2$ nanosheet–graphene networks as efficient electrocatalysts for the hydrogen evolution reaction, J. Mater. Chem. A 3 (2015) 16337–16347.
[37] B.Q. Xie, Y. Chen, M.Y. Yu, T. Sun, L.H. Lu, T. Xie, et al., Hydrothermal synthesis of layered molybdenum sulfide/N-doped graphene hybrid with enhanced supercapacitor performance, Carbon 99 (2016) 35–42.
[38] X.P. Wang, L.X. Lv, Z.H. Cheng, J. Gao, L.Y. Dong, C.G. Hu, et al., High-density monolith of N-Doped holey graphene for ultrahigh volumetric capacity of Li-Ion batteries, adv, Energy Mater. 6 (2016) 1502100.
[39] Z.Y. Wu, X.X. Xu, B.C. Hu, H.W. Liang, Y. Lin, L.F. Chen, et al., Iron carbide nanoparticles encapsulated in mesoporous Fe-N-Doped carbon nanofibers for efficient electrocatalysis, Angew. Chem. Int. Ed. 54 (2015) 8179–8183.
[40] M. Chhowalla, H.S. Shin, G. Eda, L.J. Li, K.P. Loh, H. Zhang, The chemistry of two-dimensional layered transition metal dichalcogenide nanosheets, Nat. Chem. 5 (2013) 263–275.
[41] U.N. Maiti, W.J. Lee, J.M. Lee, Y. Oh, J.Y. Kim, J.E. Kim, et al., 25th anniversary article: chemically modified/doped carbon nanotubes & graphene for optimized nanostructures & nanodevices, Adv. Mater. 26 (2014) 40–67.
[42] H.B. Wang, T. Maiyalagan, X. Wang, Review on recent progress in nitrogen-doped graphene: synthesis, characterization, and its potential applications, ACS Catal. 2 (2012) 781–794.
[43] W.S. Hummers, R.E. Offeman, Preparation of graphitic oxide, J. Am. Chem. Soc. 80 (1958), 1339-1339.
[44] Y. Yan, B.Y. Xia, X.M. Ge, Z.L. Liu, J.Y. Wang, X. Wang, Ultrathin MoS_2 nanoplates with rich active sites as highly efficient catalyst for hydrogen evolution, ACS Appl. Mater. Interfaces 5 (2013) 12794–12798.
[45] A.P. Liu, L. Zhao, J.M. Zhang, L.X. Lin, H.P. Wu, Solvent-assisted oxygen incorporation of vertically aligned MoS_2 ultrathin nanosheets decorated on reduced graphene oxide for improved electrocatalytic hydrogen evolution, ACS Appl. Mater. Interfaces 8 (2016) 25210–25218.
[46] M. Yuan, A.P. Liu, M. Zhao, W.J. Dong, T.Y. Zhao, J.J. Wang, et al., Bimetallic PdCu nanoparticle decorated three-dimensional grapheme hydrogel for non-enzymatic amperometric glucose sensor, Sens. Actuat. B-Chem. 190 (2014) 707–714.
[47] G.C. Huang, T. Chen, W.X. Chen, Z. Wang, K. Chang, L. Ma, et al., Graphene-like MoS_2/graphene composites: cationic surfactant-assisted hydrothermal synthesis and electrochemical reversible storage of lithium, Small 9 (2013) 3693–3703.
[48] Y. Hou, B. Zhang, Z.H. Wen, S.M. Cui, X.R. Guo, Z. He, et al., A 3D hybrid of layered MoS_2/nitrogen-doped graphene nanosheet aerogels: an effective catalyst for hydrogen evolution in microbial electrolysis cells, J. Mater. Chem. A 2 (2014) 13795–13800.
[49] Y. Qin, J. Yuan, J. Li, D.C. Chen, Y. Kong, F.Q. Chu, et al., Crosslinking graphene oxide into robust 3D porous N-Doped graphene, Adv. Mater. 27 (2015) 5171–5175.
[50] Y.J. Tang, Y. Wang, X.L. Wang, S.L. Li, W. Huang, L.Z. Dong, et al., Molybdenum disulfide/nitrogen-doped reduced graphene oxide nanocomposite with enlarged interlayer spacing for electrocatalytic hydrogen evolution, adv, Energy Mater. 6 (2016) 1600116.
[51] D.H. Lee, W.J. Lee, S.O. Kim, Highly efficient vertical growth of wall-number-selected, N-Doped carbon nanotube arrays, Nano Lett. 9 (2009) 1427–1432.
[52] Y. Yan, B.Y. Xia, Z.C. Xu, X. Wang, Recent development of molybdenum sulfides as advanced electrocatalysts for hydrogen evolution reaction, ACS Catal. 4 (2014) 1693–1705.
[53] M.R. Gao, J.X. Liang, Y.R. Zheng, Y.F. Xu, J. Jiang, Q. Gao, et al., An efficient molybdenum disulfide/cobalt diselenide hybrid catalyst for electrochemical hydrogen generation, Nat. Commun. 6 (2015) 5982–5988.
[54] Y.F. Zhang, L.Z. Zuo, Y.P. Huang, L.S. Zhang, F.L. Lai, W. Fan, et al., In-situ growth of few-layered MoS_2 nanosheets on highly porous carbon aerogel as advanced electrocatalysts for hydrogen evolution reaction, ACS Sustain. Chem. Eng. 3 (2015) 3014–3148.
[55] S.P. Zhang, B.V.R. Chowdari, Z.Y. Wen, J. Jin, J.H. Yang, Constructing highly oriented configuration by few-layer MoS_2: toward high-performance lithium-ion batteries and hydrogen evolution reactions, ACS Nano 9 (2015) 12464–12472.
[56] D. Merki, S. Fierro, H. Vrubel, X.L. Hu, Amorphous molybdenum sulfide films as catalysts for electrochemical hydrogen production in water, Chem. Sci. 2 (2011) 1262–1267.